Computational and Theoretical Chemistry 1188 (2020) 112949

Contents lists available at ScienceDirect

Computational and Theoretical Chemistry

journal homepage: www.elsevier.com/locate/comptc

# Theoretical investigation on anti-sandwich beryllium-boron clusters $Be_{2m}B_n$ ($m$ = 1–3): Fluxionality and multi-aromaticity

Xinlei Yu, Chang Xu, Longjiu Cheng

*Department of Chemistry, Key Laboratory of Functional Inorganic Materials of Anhui Province, Anhui University, Hefei, Anhui 230601, PR China*

ARTICLE INFO

*Keywords:*
Beryllium-boron binary cluster
Anti-sandwich
Aromaticity
Structural fluxionality

ABSTRACT

Recently, a kind of anti-sandwich beryllium doped boron clusters with middle boron ring and beryllium units on both sides have been experimentally obtained. These clusters attract our interests due to their special three layers geometry with structural fluxionality and aromaticity. Therefore, the anti-sandwich $Be_{2m}B_n$ ($m$ = 1–3) clusters are theoretically investigated in this paper to get a general view of this series of beryllium-boron binary systems. The results indicate that all these clusters possessed three-layer geometries after optimization, whose stability is demonstrated by diverse multi-aromaticity. Among these structures, $Be_4B_{10}^{2+}$ could be viewed as an analogue of naphthalene depending on its pattern of delocalized π electrons, and $Be_6B_{12}$ has a distorted boron plane and high fluxionality with potential applications as a 3D Wankel motor. Our study further reveals structural rules of anti-sandwich beryllium-boron binary clusters and enriches their structural diversity.

## 1. Introduction

Due to the electron-deficient [1–4] character of boron atom, boron clusters exhibit diverse geometric structures and special chemical properties, which attracts much attention [5–8]. During the past decades, a number of all-boron structures [9–18] have been systematically investigated using photoelectron spectroscopy (PES) [19] combined with quantum chemistry calculations, including quasi-planar, double ring and multiple ring, tubular and fullerene-like forms [20–25]. Theoretical investigations reveal that multi-center bonding systems and special aromaticity [26,27] are all in these structures, indicating their potential applications as inorganic materials.

Binary alloy clusters have rich structural and electronic properties due to their flexible tenability, which have become an active area of research in both science and technology [28–30]. Boron longs for extra electrons from other electron donor atom to produce various doped binary alloy clusters [31–42]. For metal-doped boron clusters [43], the delocalized orbitals of boron motif could interact with $d$ orbitals in metal atoms, which made the cluster stable. Interestingly, the ferrocene-like $B_{12}$·Cr·$B_{12}$ cluster introduced by our group [44] exhibits a special sandwich structure and a π-$d$-π interaction system. For nonmetallic doped boron clusters, of particular intriguing compounds are beryllium doped clusters [45–49]. An increasing number of binary beryllium-boron clusters were found both experimentally and theoretically and an intriguing triple-layered structure are investigated [50–53]. In 2016, Cui et al. [45] stumbled upon two boron-based anti-sandwich clusters $Be_2B_7^-$ and $Be_2B_8$ with the shortest Be-Be bond through PES research, which is the earliest three-layered Be-B structure. Then, Zhai group [50,51] characterized $Be_6B_{10}^{2-}$ and $Be_6B_{11}^-$ clusters, which have an aromatic anti-sandwich structure with dynamic structural fluxionality [54–56].

The special three-layered structures of these beryllium-boron clusters with aromatic character arouse our interests. In order to reveal the nature of their geometric and electronic structures, we carry out the study on a series of beryllium-boron anti-sandwich clusters $Be_{2m}B_n$ ($m$ = 1–3), composing of beryllium atoms on both sides and a middle boron plane. The structures are optimized by density functional theory (DFT) calculations, and the electronic structures are investigated to reveal the aromatic and fluxional characters. Among them, $Be_4B_{10}$ has a naphthalene-like [57,58] electronic structure and $Be_6B_{12}$ with distorted boron plane could be viewed as a 3D Wankel motor with dual fluxionality of the structure.

## 2. Methods

The B–Be binary systems $Be_{2m}B_n$ ($m$ = 1–3) are optimized using DFT methods using the PBE0 functional [59] with the 6-311G* basis set. Further energies and frequency calculations are all performed at the same level of theory. Frequency verifications show that these structures have no virtual frequencies. The PBE0 functional has been proven to be reliable for all boron and doped boron clusters [60–62]. Furthermore, the natural charges from natural population analysis (NPA) and

*E-mail addresses:* xuchang1986@ahu.edu.cn (C. Xu), clj@ustc.edu (L. Cheng).

https://doi.org/10.1016/j.comptc.2020.112949
Received 8 June 2020; Received in revised form 13 July 2020; Accepted 15 July 2020
Available online 22 July 2020
2210-271X/ 

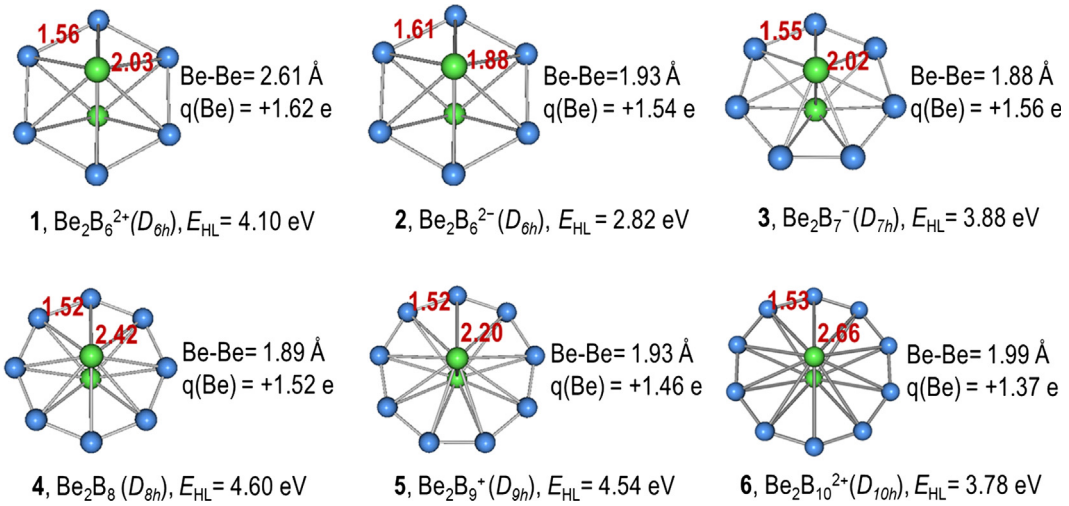


**Fig. 1.** Optimized structures of $Be_2B_n$ at the PBE0/6-311G* level of theory. The calculated bond lengths (Å), symmetries, HOMO-LUMO energy gaps and atomic partial charge of Be atoms are also labeled.

molecule orbitals (MO) are calculated to investigate the electronic characters of these clusters, while adaptive natural density partitioning (AdNDP) [63] and localized orbital locator (LOL) [64] analysis are carried out to reveal their multi-center bonding systems. All quantum chemical calculations are performed with the Gaussian 09 package [65]. Visualization of molecular orbitals is performed by Molekel 5.4 [66] and the Multiwfn [67] is used for LOL contour plots.

## 3. Results and discussions

Depending on previous experiments, geometric structures of $Be_2B_x$ ($x$ = 6–10), $Be_4B_y$ ($y$ = 8, 10) and $Be_6B_z$ ($z$ = 9–12) are built and optimized, which consists of two outer layers of beryllium units and a middle boron plane.

### 3.1. $Be_2B_n$ clusters ($n$ = 6–10)

The optimized six clusters are shown in Fig. 1, which include **1** $Be_2B_6^{2+}$ ($D_{6h}$), **2** $Be_2B_6^{2-}$ ($D_{6h}$), **3** $Be_2B_7^{-}$ ($D_{7h}$), **4** $Be_2B_8$ ($D_{8h}$), **5** $Be_2B_9^{+}$ ($D_{9h}$) and **6** $Be_2B_{10}^{2+}$ ($D_{10h}$). In these structures, two beryllium atoms are above and below the boron ring respectively. The fairly large HOMO-LUMO gaps ($E_{HL}$ = 2.82–4.60 eV) indicate their high stability. Further bond lengths and natural charges are performed to reveal electronic characters of these clusters. The calculated B-B bond lengths are within 1.52–1.61 Å, shorter than single B-B bond (1.67 Å), indicating orbital delocalization in the middle boron ring. However, the distances between top and bottom Be atoms are even shorter than 2.0 Å (2.53 Å for neutral $Be_2$, 2.25 Å for cation $Be_2^{+}$) except for **1**. Moreover, the Be atoms carry large positive charges from + 1.37e (**6**, $Be_2B_{10}^{2+}$) to + 1.62e (**1**, $Be_2B_6^{2+}$), indicating strong charge donations from $Be_2$ to boron ring due to electron deficiency of boron.

For $[Be_2B_6]^{2+}$ (**1**) cluster, AdNDP analysis reveals that, as shown in Fig. 2a, there are six 2c-2e σ bonds in the hexatomic boron ring (ON = 1.94–1.98 |e|), and there is no bond between two beryllium atoms. The rest electrons are delocalized in one 8c-2e σ bond and three 8c-2e π bonds which exhibits double aromaticity depending on Hückel's $4n + 2$ rule. As shown in the figure, there is obvious contribution of Be orbitals to the delocalized bonds. AdNDP chemical bonding of $Be_2B_8$ (**4**) shown in Fig. 2b also indicates double aromaticity with three delocalized σ bonds and three π bonds. Similarly, clusters **2**, **3**, **5** and **6** have similar bonding patterns.

To verify the aromaticity, the nuclear independent chemical shift (NICS) [68,69]values are also calculated for these clusters in the center of boron rings (Table 1). The large negative values confirm high aromaticity of these clusters. Thus, these structures possess unusual stability with their double aromaticity of delocalized σ and π electrons.

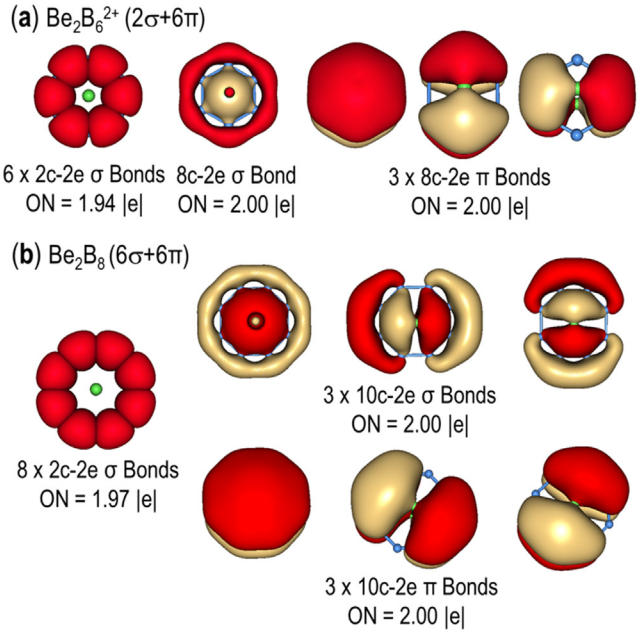


**Fig. 2.** AdNDP chemical bonding for (a) **1** $[Be_2B_6]^{2+}$ and (b) **4** $Be_2B_8$ at the PBE0/6-311G* level of theory. ON gives the occupation number.

**Table 1**
NICS values (ppm) of clusters **1–6** in the center of middle boron ring.

| $Be_2B_6^{2+}$ | $Be_2B_6^{2-}$ | $Be_2B_7^{-}$ | $Be_2B_8$ | $Be_2B_9^{+}$ | $Be_2B_{10}^{2+}$ |
|---|---|---|---|---|---|
| −53.73 | −36.02 | −37.15 | −34.31 | −32.79 | −31.33 |

### 3.2. $Be_4B_n$ clusters ($n$ = 8,10)

The optimized structures of clusters **7** $Be_4B_8$ ($D_{2h}$) and **8** $Be_4B_{10}^{2+}$ ($D_{2h}$) with $Be_2$ units at both sides of boron ring are shown in Fig. 3. Cluster **7** has a large HOMO-LUMO gap (2.27 eV), and the lightly short distance between two beryllium atoms on the same layer indicate certain interaction. AdNDP bonding in Fig. 3c reveals that the $Be_2$ units are involved in two 6c-2e σ bonds respectively. NICS plane shown in Fig. 3a

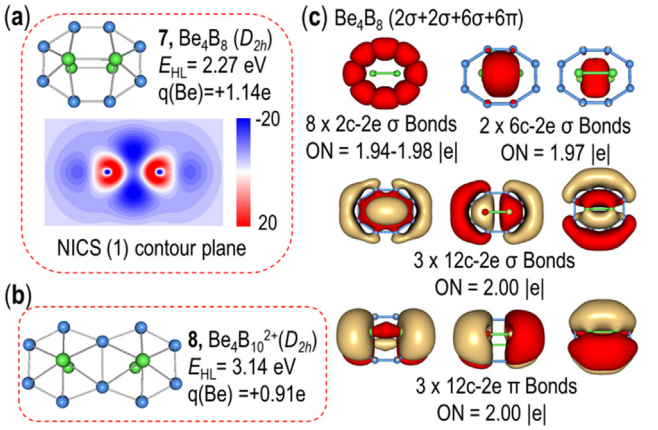


**Fig. 3.** Structures, HOMO-LUMO energy gaps, natural charges for Be atoms of (a) **7** and (b) **8**, and (c) AdNDP chemical bonding of **7**. NICS (1) contour planes in (a) is 1.0 Å above the boron plane. Bond length of **7**: B-B = 1.53–1.82, B-Be = 1.86–2.07 and Be-Be = 1.93–2.47; **8**: B-B = 1.54–1.66, B-Be = 1.89–2.07 and Be-Be = 2.33–2.89, labeled in Å.

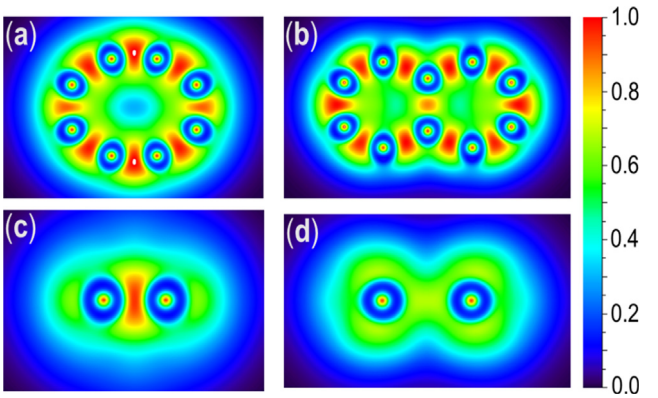


**Fig. 4.** Localized orbital locator (LOL) contour plots for cluster **7** (a) boron ring plan (c) beryllium plane paralleling to boron plane and **8** (b) boron ring plan (d) beryllium plane. LOL values below 0.5 (blue to green) indicate delocalized electron, above 0.5 (yellow to red) characterize localized electrons.

reveals the aromaticity induced by these delocalized bonds. Moreover, there are also three 12c-2e σ and three π bonds, indicating four-fold σ/π aromaticity (2σ/2σ/6σ/6π). Finally, localized orbital locator (LOL) contour plots for beryllium plane also indicate strong covalent interactions (Fig. 4).

Along with the expanded boron ring, the distance between two beryllium atoms increases (2.89 Å), and boron ring are separated into two parts in $[Be_4B_{10}]^{2+}$ (**8**). The geometric structure indicates few interactions between beryllium atoms, which could also be confirmed in LOL results in Fig. 4. Furthermore, results of AdNDP chemical bonding show that $[Be_4B_{10}]^{2+}$ (**8**) is analogous of naphthalene in π electrons (Fig. 5). There are 6c-2e σ bonds in each part of **8** which fellow Hückel's rule respectively. The rest 10 electrons are delocalized over whole cluster, and the shape of these five delocalized orbital are corresponding to the delocalized systems of naphthalene molecule. Further NICS calculations shown in Fig. 6 reveal their aromaticity and confirmed the similarity of the electronic systems with 10 π electrons.

### 3.3. $Be_6B_n$ clusters ($n$ = 9–12)

When the number of beryllium atoms increase to three in each sides, the peripheral boron ring should be large enough to form a stable structure. Several stable structures with large size boron ring are obtained: **9** $Be_6B_9^+$ ($D_{3h}$), **10** $Be_6B_{10}^{2+}$ ($C_{2v}$), **11** $Be_6B_{10}^{2-}$ ($C_{2v}$), **12** $Be_6B_{11}^-$ ($C_{2v}$) and **13** $Be_6B_{12}$ ($D_{3h}$), as shown in Figs. 7 and 8. The obtained $C_{2v}$ geometry of **11** and **12** are in accord with previous works [50,51], and all these clusters have similar geometric character. Natural atomic charge value suggests that the two $Be_3$ units collectively donate a net charge of more than 8|e| to the boron ring. WBI bond order (0.03–0.08) between two beryllium atoms on upper and lower layers suggests that there is no interaction existed between two $Be_3$ rings.

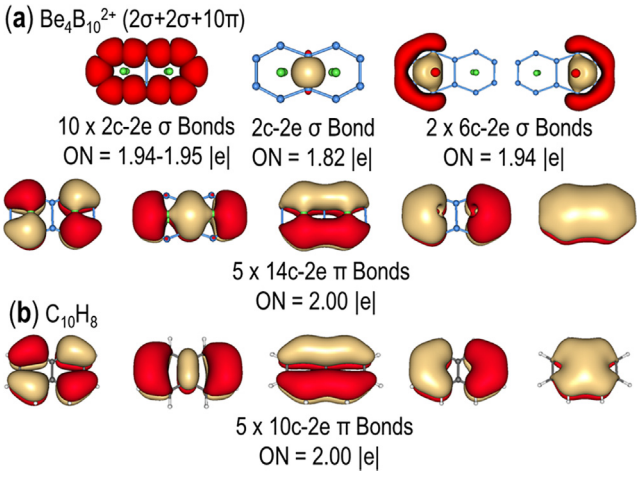


**Fig. 5.** AdNDP chemical bonding of (a) **8** and (b) naphthalene ($C_{10}H_8$).

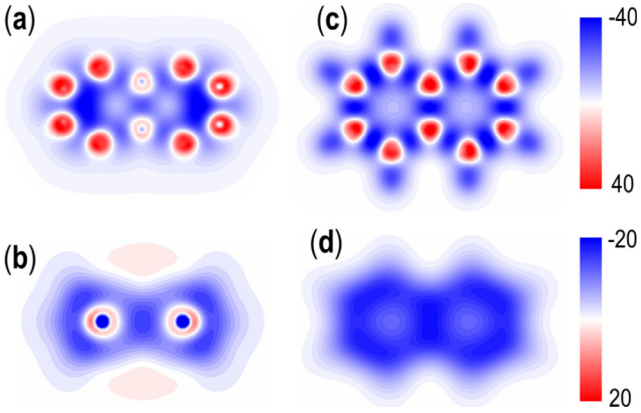


**Fig. 6.** (a) NICS values of boron plane and (b) NICS(1) plane above the boron plane at 1.0 Å for $[Be_4B_{10}]^{2+}$ (**8**); (c) NICS and (d) NICS(1) for $C_{10}H_8$.

Further AdNDP results in Fig. 7 reveal that there is a 3c-2e delocalized σ bond in each $Be_3$ ring in these clusters. Moreover, 16 delocalized electrons in **9** possesses three 15c-2e σ bonds and five 15c-2e π bonds, 20 delocalized electron in cluster **11** generates five 16c-2e σ bonds and five 16c-2e π bonds. AdNDP bonding patterns of **10** and **12** are similar to **9** and **11** respectively. Finally, the quite negative NICS values of these clusters in the center of boron ring also confirm very similar aromaticity of these clusters (Supporting Information, Table S1).

Bonding systems of cluster **13** is similar as **11** and **12** with same number of valence electrons, and the AdNDP bonding patterns are shown in Fig. S2. However, when one $Be_3$ ring rotated and two $Be_3$ units become staggered conformation, something interesting happened. The boron ring distorts and becomes quasi-planar to enhance the coulomb attraction between Be atoms and boron ring. The staggered conformation **14** $Be_6B_{12}$ ($D_{3d}$) is more stable as shown in Fig. 8a, which has a larger HOMO-LUMO gap and is 1.61 kcal/mol lower in energy than **13** ($D_{3h}$).

In order to reveal the bonding character in **14**, their bond lengths are calculated. First, the B-B bonds length in the $B_{12}$ ring (1.53 Å) are beyond single bond, showing a character of double bond. Then, the Be-

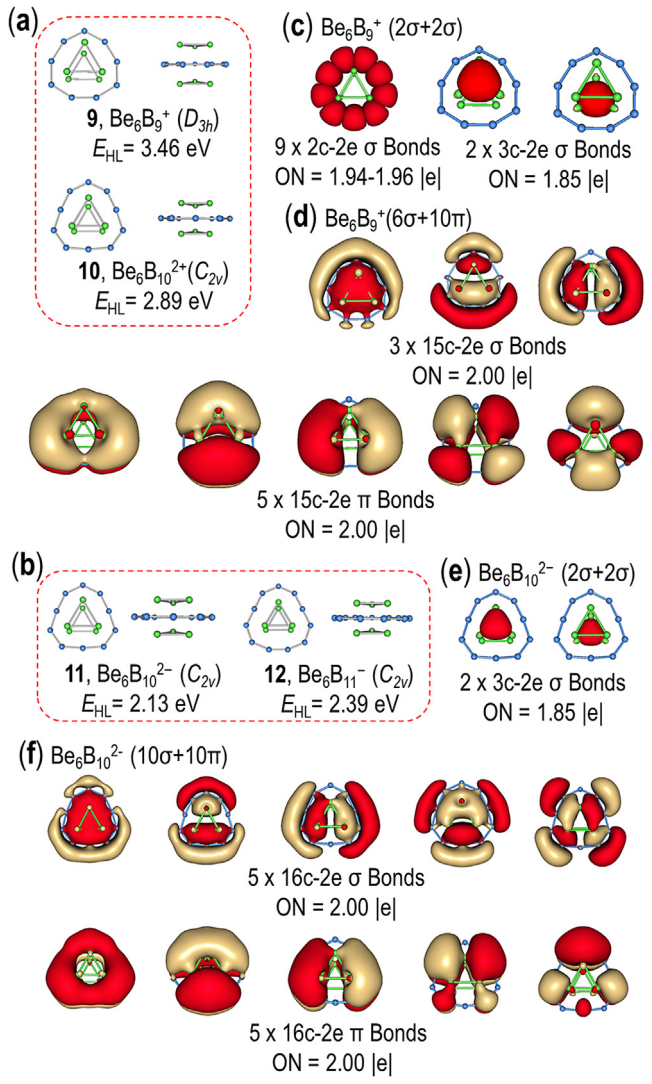


**Fig. 7.** Structures, HOMO-LUMO energy gaps, symmetries of (a) **9**, **10** and (b) **11**, **12**; AdNDP chemical bonding of (c) (d) **9**, and (e) (f) **11.**

Be distances in $Be_3$ subsystems (2.31 Å) suggest strong interaction, equivalent to that of neutral $Be_2$ (2.53 Å), otherwise two $Be_3$ rings have no interaction with each other. The natural atomic charges of cluster **14** indicate substantial interlayer charge transfers from the two $Be_3$ subsystems to the outer $B_{12}$ ring and each beryllium atom carries a positive charge of 1.23 |e|, that is, six Be atoms collectively donate a net charge of 7.23 |e| to the $B_{12}$ ring. In addition, molecule orbitals (MO) calculations give a straightforward description of its chemical bonding (Supporting Information, Fig. S3), consistent with subsequent AdNDP analysis.

AdNDP analysis reveals that there are twelve B-B bonds and two 3c-2e σ bonds in **14** as shown in Fig. 8b. Further LOL contour plots in Fig. 9a confirm the strong interactions between boron atoms, while LOL in Fig. 9b of beryllium ring reveals a three-center bond for each $Be_3$ units with LOL values around 0.8 characterize localized electrons. The rest twenty valence electrons generate five 18c-2e σ bonds and five π bonds (Fig. 8b) indicating double aromaticity. This aromaticity also suggested by NICS results in Fig. 9c and 9d. For the whole anti-sandwich cluster, combined with two-electron subsystem in each $Be_3$ ring and 10σ and 10π electrons subsystems in the $B_{12}$ ring, it render 2σ/2σ/10σ/10π quadruple aromaticity.

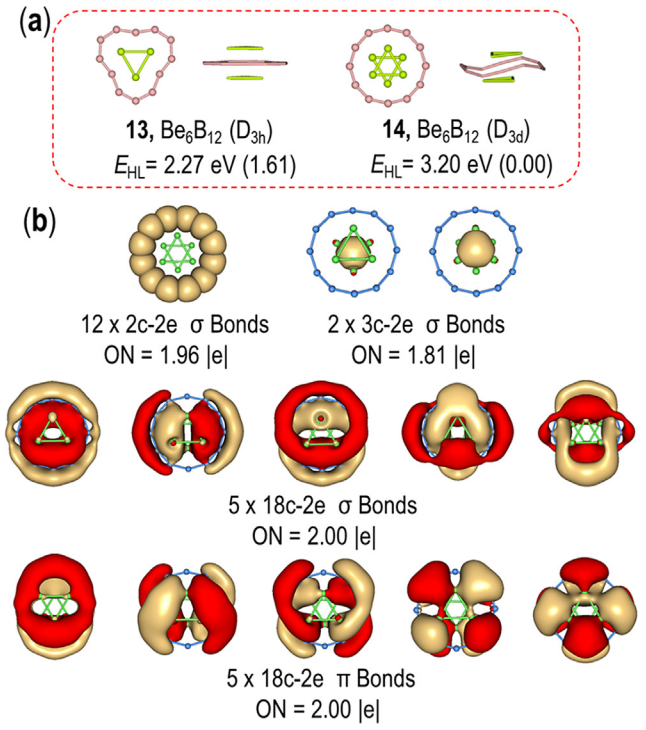


**Fig. 8.** (a) Structures, HOMO-LUMO energy gaps, symmetries of **13**, **14**, and (b) AdNDP chemical bonding of **14.**

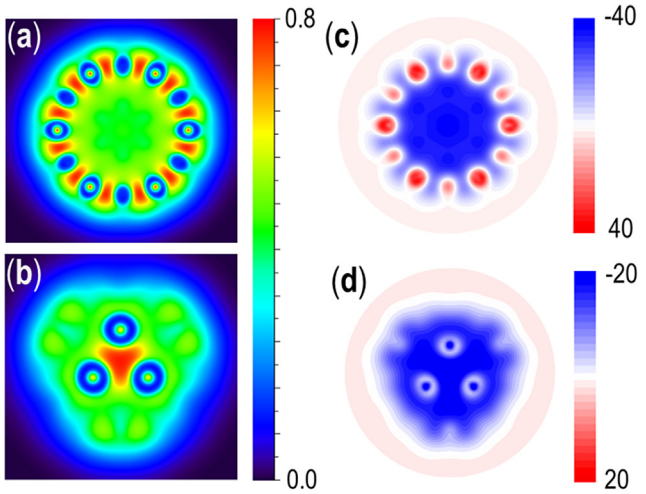


**Fig. 9.** LOL contour plots for cluster **14** (a) boron ring plane; (b) beryllium ring plane; NICS values of (c) boron plane and (d) 1.0 Å above the boron plane.

### *3.4. Structural fluxionality of $Be_6B_{12}$ cluster*

Due to the special geometry of $Be_6B_n$ cluster which composed of relative independent inner $Be_6$ unit and outside $B_n$ ring, it could be inferred that they have structural character of molecular wheel. Herein, clusters $Be_6B_{12}$ are described as an example for their rotation and distortion characteristics in detail. Transition states between the $D_{3d}$ (**14**) and $D_{3h}$ (**13**) $Be_6B_{12}$ clusters are located through rotating the entire $Be_6$ unit or twisting one of the beryllium triangular prism (Fig. 10). Subsequently, rotated **TS1** and twisted **TS2** are sought out, indicating attractive fluxionality for cluster $Be_6B_{12}$. The revolution barrier of cluster **14** is 0.69 kcal/mol, while the energy barrier for the twisting mode is calculated to be 8.30 kcal/mol.

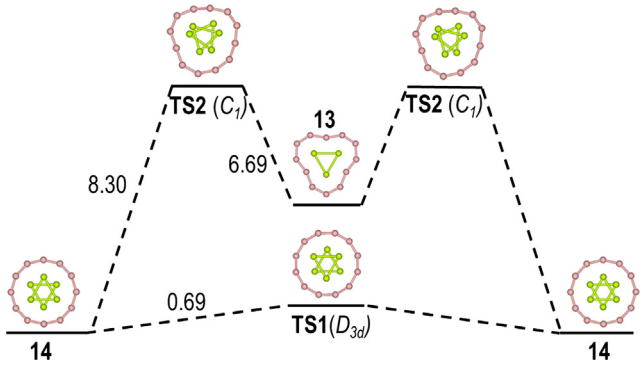


**Fig. 10.** Energy pathways for two configurations of the $Be_6B_{12}$ cluster (**13** and **14**). **TS1** and **TS2** are the transition state whose symmetries are in parentheses. The relative energy is given in kcal/mol.

## 4. Conclusion

In this paper, a series of anti-sandwich beryllium-boron clusters are optimized and theoretically investigated to reveal the rules of their geometric and electronic characters. The results indicate strong charge donations from side beryllium atoms to the middle boron ring, which induce fluxionality and multi-aromaticity. For $Be_4B_n$ clusters ($n$ = 8, 10), two $Be_2$ subsystems share two electrons, while outer boron ring exhibits double σ/π aromaticity, which presents a four-fold aromaticity. Depending on the electronic character, $Be_4B_{10}^{2+}$ is an analogue of naphthalene with double σ/π aromaticity, though there is nonbonding between beryllium atoms. The $Be_6B_n$ clusters ($n$ = 9–12) also possess four-fold aromaticity as two $Be_3$ rings share two electrons respectively. Specially, boron plane distorts in $D_{3d}$ $Be_6B_{12}$ which could be viewed as 3D Wankel motor with dual fluxionality of structure. This work gives a general perspective for anti-sandwich beryllium-boron binary systems, which gives references for design of boron based functional materials.

## CRediT authorship contribution statement

**Xinlei Yu:** Methodology, Software, Writing - original draft. **Chang Xu:** Writing - review & editing. **Longjiu Cheng:** Supervision.

## Declaration of Competing Interest

The authors declare that they have no known competing financial interests or personal relationships that could have appeared to influence the work reported in this paper.

## Acknowledgment

This work is financed by the National Natural Science Foundation of China (Grant 21873001), and by the Foundation of Distinguished Young Scientists of Anhui Province. The calculations are carried out at the High-Performance Computing Center of Anhui University.

## Appendix A. Supplementary material

Supplementary data to this article can be found online at https://doi.org/10.1016/j.comptc.2020.112949.

## References

[1] A.J. Mannix, X.-F. Zhou, B. Kiraly, J.D. Wood, D. Alducin, B.D. Myers, X. Liu, B.L. Fisher, U. Santiago, J.R. Guest, Science 350 (2015) 1513–1516.
[2] A.P. Sergeeva, I.A. Popov, Z.A. Piazza, W.-L. Li, C. Romanescu, L.-S. Wang, A.I. Boldyrev, Acc. Chem. Res. 47 (2014) 1349–1358.
[3] C. Romanescu, T.R. Galeev, W.-L. Li, A.I. Boldyrev, L.-S. Wang, J. Chem. Phys. 138 (2013) 134315.
[4] H.T. Pham, L. Van Duong, B.Q. Pham, M.T. Nguyen, Chem. Phys. Lett. 577 (2013) 32–37.
[5] E. Oger, N.R. Crawford, R. Kelting, P. Weis, M.M. Kappes, R. Ahlrichs, Angew. Chem. Int. Ed. 46 (2007) 8503–8506.
[6] L. Cheng, J. Chem. Phys. 136 (2012) 104301.
[7] L. Ren, L. Cheng, Y. Feng, X. Wang, J. Chem. Phys. 137 (2012) 014309.
[8] B. Albert, H. Hillebrecht, Angew. Chem. Int. Ed. 48 (2009) 8640–8668.
[9] L. Li, L. Cheng, J. Chem. Phys. 138 (2013) 094312.
[10] X. Dong, S. Jalife, A. Vásquez-Espinal, J. Barroso, M. Orozco-Ic, E. Ravell, J.L. Cabellos, W.-Y. Liang, Z.-H. Cui, G. Merino, Nanoscale 11 (2019) 2143–2147.
[11] A.P. Sergeeva, B.B. Averkiev, H.-J. Zhai, A.I. Boldyrev, L.-S. Wang, J. Chem. Phys. 134 (2011) 224304.
[12] T.B. Tai, A. Ceulemans, M.T. Nguyen, Chem. - Eur. J. 18 (2012) 4510–4512.
[13] F. Cervantes-Navarro, G. Martínez-Guajardo, E. Osorio, D. Moreno, W. Tiznado, R. Islas, K.J. Donald, G. Merino, Chem. Commun. 50 (2014) 10680–10682.
[14] Y.-J. Wang, X.-Y. Zhao, Q. Chen, H.-J. Zhai, S.-D. Li, Nanoscale 7 (2015) 16054–16060.
[15] Q. Chen, T.-T. Chen, H.-R. Li, X.-Y. Zhao, W.-J. Chen, H.-J. Zhai, S.-D. Li, L.-S. Wang, Nanoscale 11 (2019) 9698–9704.
[16] T. BaáTai, M. ThoáNguyen, Chem. Commun. 52 (2016) 1653–1656.
[17] H.T. Pham, L.V. Duong, N.M. Tam, M.P. Pham-Ho, M.T. Nguyen, Chem. Phys. Lett. 608 (2014) 295–302.
[18] A.N. Alexandrova, A.I. Boldyrev, H.-J. Zhai, L.-S. Wang, Coord. Chem. Rev. 250 (2006) 2811–2866.
[19] L.-S. Wang, Int. Rev. Phys. Chem. 35 (2016) 69–142.
[20] S. Li, Z. Zhang, Z. Long, G. Sun, S. Qin, Sci. Rep. 6 (2016) 25020.
[21] Y. Yuan, L. Cheng, J. Chem. Phys. 137 (2012) 044308.
[22] J. Zhao, X. Huang, R. Shi, H. Liu, Y. Su, R.B. King, Nanoscale 7 (2015) 15086–15090.
[23] J. Lv, Y. Wang, L. Zhu, Y. Ma, Nanoscale 6 (2014) 11692–11696.
[24] Z. Zhang, Y. Yang, G. Gao, B.I. Yakobson, Angew. Chem. Int. Ed. 54 (2015) 13022–13026.
[25] E.S. Penev, S. Bhowmick, A. Sadrzadeh, B.I. Yakobson, Nano Lett. 12 (2012) 2441–2445.
[26] A.I. Boldyrev, L.-S. Wang, Phys. Chem. Chem. Phys. 18 (2016) 11589–11605.
[27] W.-L. Li, Q. Chen, W.-J. Tian, H. Bai, Y.-F. Zhao, H.-S. Hu, J. Li, H.-J. Zhai, S.-D. Li, L.-S. Wang, J. Am. Chem. Soc. 136 (2014) 12257–12260.
[28] B.-Y. Song, Y. Zhou, H.-M. Yang, J.-H. Liao, L.-M. Yang, X.-B. Yang, E. Ganz, J. Am. Chem. Soc. 141 (2019) 3630–3640.
[29] L.-M. Yang, V. Bacic, I.A. Popov, A.I. Boldyrev, T. Heine, T. Frauenheim, E. Ganz, J. Am. Chem. Soc. 137 (2015) 2757–2762.
[30] L.-M. Wen, G.-L. Li, L.-M. Yang, H. Pan, E. Ganz, Mater. Today. Commun. 24 (2020) 100914.
[31] H. Bai, H.-J. Zhai, S.-D. Li, L.-S. Wang, Phys. Chem. Chem. Phys. 15 (2013) 9646–9653.
[32] L. Liu, D. Moreno, E. Osorio, A.C. Castro, S. Pan, P.K. Chattaraj, T. Heine, G. Merino, RSC Adv. 6 (2016) 27177–27182.
[33] H.J. Zhai, A.N. Alexandrova, K.A. Birch, A.I. Boldyrev, L.S. Wang, Angew. Chem. Int. Ed. 42 (2003) 6004–6008.
[34] H.T. Pham, K.Z. Lim, R.W. Havenith, M.T. Nguyen, Phys. Chem. Chem. Phys. 18 (2016) 11919–11931.
[35] L. Cheng, C. Ren, X. Zhang, J. Yang, Nanoscale 5 (2013) 1475–1478.
[36] C. Xu, L. Cheng, J. Yang, J. Chem. Phys. 141 (2014) 124301.
[37] H. Ren, H. Shao, L. Zhang, D. Guo, Q. Jin, R. Yu, L. Wang, Y. Li, Y. Wang, H. Zhao, Adv. Energy Mater. 5 (2015) 1500296.
[38] L. del Olmo, C. Morera-Boado, R. López, J.M.G. de la Vega, J. Mol. Model. 20 (2014) 2175.
[39] M.K. Si, B. Ganguly, New J. Chem. 40 (2016) 9132–9138.
[40] D. Naglav, B. Tobey, A. Neumann, D. Bläser, C. Wölper, S. Schulz, Organometallics 34 (2015) 3072–3078.
[41] Q. Liu, L. Cheng, J. Alloys Compd. 771 (2019) 762–768.
[42] Q. Zheng, C. Xu, X. Wu, L. Cheng, ACS Omega 3 (2018) 14423–14430.
[43] T.R. Galeev, C. Romanescu, W.L. Li, L.S. Wang, A.I. Boldyrev, Angew. Chem. Int. Ed. 51 (2012) 2101–2105.
[44] Y. Yuan, L. Cheng, J. Chem. Phys. 138 (2013) 024301.
[45] W.L. Li, Y.F. Zhao, H.S. Hu, J. Li, L.S. Wang, Angew. Chem. Int. Ed. 53 (2014) 5540–5545.
[46] Z.A. Piazza, H.-S. Hu, W.-L. Li, Y.-F. Zhao, J. Li, L.-S. Wang, Nat. Commun. 5 (2014) 3113.
[47] Z.H. Cui, W.S. Yang, L. Zhao, Y.H. Ding, G. Frenking, Angew. Chem. Int. Ed. 128 (2016) 7972–7977.
[48] X. Dong, S. Jalife, A. Vásquez-Espinal, E. Ravell, S. Pan, J.L. Cabellos, W.Y. Liang, Z.H. Cui, G. Merino, Angew. Chem. Int. Ed. 57 (2018) 4627–4631.
[49] W.-L. Li, X. Chen, T. Jian, T.-T. Chen, J. Li, L.-S. Wang, Nat. Rev. Chem. 1 (2017) 0071.
[50] J.C. Guo, L.Y. Feng, Y.J. Wang, S. Jalife, A. Vásquez-Espinal, J.L. Cabellos, S. Pan, G. Merino, H.J. Zhai, Angew. Chem. Int. Ed. 56 (2017) 10174–10177.
[51] L.-Y. Feng, J.-C. Guo, P.-F. Li, H.-J. Zhai, Phys. Chem. Chem. Phys. 20 (2018) 22719–22729.
[52] S. Đorđević, S. Radenković, Phys. Chem. Chem. Phys. 21 (2019) 7105–7114.
[53] Y.-J. Wang, C.-Q. Miao, J.-J. Xie, Y.-R. Wei, G.-M. Ren, New J. Chem. 43 (2019) 15979–15982.
[54] J.O.C. Jiménez-Halla, R. Islas, T. Heine, G. Merino, Angew. Chem. Int. Ed. 49 (2010) 5668–5671.
[55] J. Zhang, A.P. Sergeeva, M. Sparta, A.N. Alexandrova, Angew. Chem. Int. Ed. 51 (2012) 8512–8515.

[56] S. Jalife, L. Liu, S. Pan, J.L. Cabellos, E. Osorio, C. Lu, T. Heine, K.J. Donald, G. Merino, Nanoscale 8 (2016) 17639–17644.
[57] A.P. Sergeeva, Z.A. Piazza, C. Romanescu, W.-L. Li, A.I. Boldyrev, L.-S. Wang, J. Am. Chem. Soc. 134 (2012) 18065–18073.
[58] W. Huang, A.P. Sergeeva, H.-J. Zhai, B.B. Averkiev, L.-S. Wang, A.I. Boldyrev, Nat. Chem. 2 (2010) 202.
[59] C. Adamo, V. Barone, J. Chem. Phys. 110 (1999) 6158–6170.
[60] J.-D. Chai, S.-P. Mao, Chem. Phys. Lett. 538 (2012) 121–125.
[61] J.M. del Campo, J.L. Gázquez, S. Trickey, A. Vela, J. Chem. Phys. 136 (2012) 104108.
[62] J. Zhao, L. Wang, F. Li, Z. Chen, J. Phys. Chem. A 114 (2010) 9969–9972.
[63] D. Zubarev, A. Boldyrev, Phys. Chem. Chem. Phys. 10 (2008) 5207.
[64] H.L. Schmider, A.D. Becke, J. Mol. Struct: THEOCHEM 527 (2000) 51.
[65] M.J. Frisch, G.W. Trucks, H.B. Schlegel, G.E. Scuseria, M.A. Robb, J.R. Cheeseman, J.A. Montgomery, Jr., T. Vreven, K.N. Kudin, J.C. Burant, J.M. Millam, S.S. Iyengar, J. Tomasi, V. Barone, B. Mennucci, M. Cossi, G. Scalmani, N. Rega, G.A. Petersson, H. Nakatsuji, M. Hada, M. Ehara, K. Toyota, R. Fukuda, J. Hasegawa, M. Ishida, T. Nakajima, Y. Honda, O. Kitao, H. Nakai, M. Klene, X. Li, J.E. Knox, H.P. Hratchian, J.B. Cross, V. Bakken, C. Adamo, J. Jaramillo, R. Gomperts, R.E. Stratmann, O. Yazyev, A.J. Austin, R. Cammi, C. Pomelli, J.W. Ochterski, P.Y. Ayala, K. Morokuma, G.A. Voth, P. Salvador, J.J. Dannenberg, V.G. Zakrzewski, S. Dapprich, A.D. Daniels, M.C. Strain, O. Farkas, D.K. Malick, A.D. Rabuck, K. Raghavachari, J. B. Foresman, J.V. Ortiz, Q. Cui, A.G. Baboul, S. Clifford, J. Cioslowski, B.B. Stefanov, G. Liu, A. Iashenko, P. Piskorz, I. Komaromi, R.L. Martin, D.J. Fox, T. Keith, M.A. Al-Laham, C.Y. Peng, A. Nanayakkara, M. Challacombe, P.M.W. Gill, B. Johnson, W. Chen, M.W. Wong, C. Gonzalez, J.A. Pople, Gaussian 09. Wallingford, 2009.
[66] U. Varetto, MOLEKEL 5.4, Swiss National Supercomputing Centre, Manno, Switzerland, 2009.
[67] T. Lu, F. Chen, J. Comput. Chem. 33 (2012) 580–592.
[68] P.V.R. Schleyer, C. Maerker, A. Dransfeld, H. Jiao, N.J. van Eikema Hommes, J. Am. Chem. Soc. 118 (1996) 6317–6318.
[69] L.-Y. Feng, R. Li, H.-J. Zhai, Phys. Chem. Chem. Phys. 21 (2019) 20523–20537.